Solvation Free Energy Reaction Curves for Electron Transfer in Aqueous Solution: Theory and Simulation

Robert B. Yelle and Toshiko Ichiye*

Departments of Biochemistry/Biophysics and of Chemistry, Washington State University, Pullman, Washington 99164-4660

Received: January 3, 1997[⊗]

The solvation free energy curves for electron transfer between several types of ions in aqueous solution are studied by molecular dynamics computer simulations and by simple theoretical models. By using models of increasing complexity, contributions of different physical effects are evaluated. The theoretical models are for two ions at infinite separation in a dielectric continuum: the first is based on the Born solvation free energy, which assumes a linear response of the solvent and thus is basically Marcus theory, and the second is based on a nonlinear response model of ionic solvation by Hyun, Babu, and Ichiye (HBI), which includes the effects of dielectric saturation. Finally, molecular dynamics simulations of ions at infinite and finite separations describe the molecular nature of the solvent, with the latter including the influence of the solutes on each other. The focus here is on the orientational rather than electronic polarization, although the latter also will contribute. Previously, comparison of HBI and Born free energy curves showed that nonlinearities are most pronounced in electron transfer reactions involving a neutral to charged species or vice versa and become much less evident as the magnitude of charges of the solutes increases. Here, a comparison of results for ions at infinite separation from the molecular dynamics simulations and the HBI and Born models shows that dielectric saturation greatly reduced the activation energy $\Delta G^{\ddagger}$ mainly by shifting the free energy curves closer together (*i.e.*, by reducing the polarization energy) but affected $\Delta G^{\ddagger}$ to a lesser degree by the nonparabolic nature of the curve. Moreover, it shows that the contribution of the molecular structure of water such as density variations and hydrogen bonding was to shift the curves apart, resulting in a smaller increase in $\Delta G^{\ddagger}$. In addition, a comparison of molecular dynamics results for ions at infinite and finite separation shows that the effect of bringing the ions to a close separation was to reduce $\Delta G^{\ddagger}$ mainly by the reduction of the solvent reorganization at large distances, thus shifting the curves together. The direct influence of one solute on the polarization of the other was to increase the nonparabolic nature of the curve, which affects $\Delta G^{\ddagger}$ less.

Introduction

Electron transfer reactions have been the subject of many theoretical and experimental studies. Much of the framework for current electron transfer theories was developed by Marcus[1] and Levich.[2] Marcus theory assumes that the rate of an electron transfer reaction is in part dependent on the response of the solvent to the transfer of an electron from the donor to acceptor. In the original formation, the polarization of a continuum solvent was assumed to respond linearly to changes in charge. Consequently, this model predicts that the free energy functions depend quadratically on the solvent coordinate and that the force constants describing the curvature for the products and the reactants are equal regardless of the nature of the products and reactants. This paper focuses on understanding the factors influencing the free energy curve and thus the activation energy, $\Delta G^{\ddagger}$, including nonlinearity of the solvent response, molecular interactions and influence of one solute on the solvent polarization of the other.

Since the original formalism by Marcus assumes a continuum approximation for the solvent, the description of the microscopic details of the electron transfer process is vague. Therefore, computer simulations have been done on various electron transfer systems, and free energy curves have been calculated from these simulations using methods pioneered by Warshel and co-workers.[3−6] For instance, Hwang and Warshel have studied the exchange between two benzene-like solutes,[5] and later Chandler and co-workers studied the ferric−ferrous self-exchange reaction,[7,8] both using molecular dynamics (MD) simulations. In both cases, the assumption of a parabolic free energy surface was found to be quite good, and the activation energy, $\Delta G^{\ddagger}$, calculated from the free energy curves was close to that calculated using Marcus theory. Furthermore, the force constants describing the parabolas are by definition equal for these symmetric reactions.

However, Kakitani and Mataga[9,10] pointed out in a study of a charge separation and recombination process that the motions of polar solvent molecules are more restricted around a charged solute than a neutral solute, and thus the fluctuations in the solvent coordinate of the charged pair would be lower than those of the neutral pair. Since the force constants describing the parabolic free energy curves are characterized by the fluctuations in the solvent coordinate, this implies the force constants also depend on the charged state of the reactants and products involved. Carter and Hynes[11] and King and Warshel[6] calculated free energy surfaces for a charge separation/recombination from simulations of a neutral pair, A−B, and an ion pair, $A^{+}-B^{-}$, which confirmed the hypothesis that the solvent fluctuations were larger around the neutral pair than the ion pair. However, Tachiya points out that the analysis by Carter assumed that the free energy curves are adequately described as parabolas, which cannot be correct and leads to unrealistic relations between $\Delta G^{\ddagger}$ and the solvent reorganization.[12] Our earlier study of the nonlinear behavior of the solvent free energy[13] using the Hyun,

* Author to whom correspondence should be addressed.
⊗ Abstract published in *Advance ACS Abstracts,* April 15, 1997.

S1089-5647(97)00081-3 CCC: $14.00

Babu, and Ichiye (HBI) model of ionic solvation[14] resolves the apparent inconsistency between the unequal curvatures found in the simulations and Tachiya's observations, showing that nonlinear response leads to both unequal curvatures and nonparabolic curves.

One caveat must be mentioned about the above mentioned computer simulation studies and the work presented here. The focus of most of these studies has been on the orientational polarization, *i.e.*, the polarization due to orientation of the solvent dipole moments by the electric fields due to the ions. The electronic polarization will also contribute significantly and has been the focus of studies by several workers.[15−17] However, these workers have ignored complexities in the orientational polarization by considering only a linear response model. Moreover, the vibrational polarization[5] has been generally been ignored. Some headway has been made in computer simulations that include both orientational and electronic polarization.[6] However, the neglect of electronic and vibrational polarization here is motivated by two factors. First, studying the Born and HBI models neglecting these two factors allows direct comparison with the standard water models used in computer simulations, which are nonpolarizable and rigid and thus do not allow electronic or vibrational polarization. Second and more importantly, excluding these two factors is essential in understanding orientational polarization effects because there are fewer degrees of freedom in the system. Of course, the different contributions are coupled; for instance, electronic shielding will reduce saturation effects. Thus, once the individual effects are understood, the ultimate goal is to include the important ones in the theoretical models. Already, other workers have developed polarizable models for computer simulations for various systems, including rigid[18−21] and flexible water.[22]

In this paper, we examine the physical origins of the solvation free energy by comparison of MD simulations and simple models of ionic solvation. Here, several levels of complexity of the solvent representation are considered. At the zeroth order, Marcus theory is considered in terms of the Born approximation, *i.e.*, the continuum level. The first order correction considered is the HBI theory, which gives the nonlinear response of a continuum to increasing charge of the ion. The next order of complexity is molecular dynamics simulations of the donor and acceptor at infinite separation, which describe the influence of the molecular nature of solute−solvent interactions. The highest order of complexity is of simulations of the reacting pairs at close separation, which describe the influence of one solute on the solvation of the other. Three systems are studied: a self-exchange reaction between two highly charged ions (nominally a $Fe^{2+}-Fe^{3+}$ reaction), another self-exchange reaction involving a singly-charged solute/neutral solute pair, and a charge separation/recombination reaction.

Methods

A. Electron Transfer Theory. The free energy surface for an electron transfer reaction

$$D^m + A^n \rightarrow D^{m+1} + A^{n-1}$$

is shown schematically in Figure 1, where R refers to the reactants D^m and A^n, P refers to the products D^{m+1} and A^{n-1}, and the reaction coordinate X is the degree of polarization of the solvent.

The activation free energy, $\Delta G^{\ddagger}$, can be calculated from Marcus theory by[1]

$$\Delta G^{\ddagger} = (\lambda + \Delta G^{\circ})^2/4\lambda \tag{1}$$

where ΔG° is the free energy of electron transfer and λ is the solvent reorganization energy (see Figure 1). The latter is the energy released when the solvent relaxes from configurations that are in equilibrium with respect to the reactants to configurations that are in equilibrium with respect to the products, while the charge distribution is that of the products. This relation is based on the assumption that the free energy is a quadratic function of the polarization coordinate but does not require an explicit definition of the polarization coordinate.

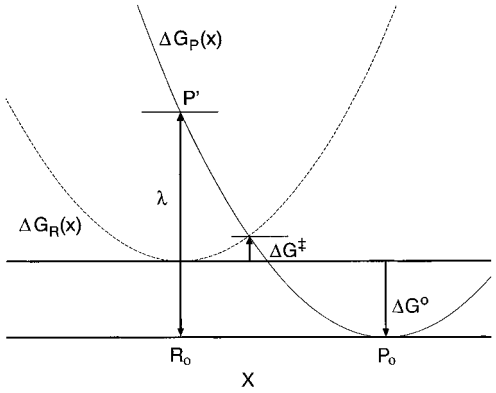

Figure 1. Reaction coordinate diagram for electron transfer reactions.

The free energy surface can be calculated from the simulation data by the relation[3]

$$\Delta G_R(X) = -k_B T \ln[P_R(X)]$$
$$\Delta G_P(X) = -k_B T \ln[P_P(X)] + \Delta G^{\circ} \tag{2}$$

where $P(X)$ is the probability of a given value of X, k_B is the Boltzmann constant, and T is the temperature. The activation free energy can also be calculated from the ratio of the probability of being at the transition state ($X = 0$) versus the probability of being in the equilibrium state ($X = X_{min}$),

$$\Delta G^{\ddagger} = -k_B T \ln[P(0)/P(X_{min})] \tag{3}$$

This definition of $\Delta G^{\ddagger}$ is thus dependent on the exact definition of X. The polarization coordinate X is defined as the difference in the potential energy, V, between the product and reactant state for the same configuration of the solvent.

$$X = \Delta V = V_P - V_R (= \Phi_D - \Phi_A) \tag{4}$$

The quantities Φ in the last equality are the electrostatic potentials at the donor and acceptor (subscripts D and A, respectively) in the tight binding approximation. We have also generalized them previously.[13]

If the distribution of X is Gaussianly distributed about X_{min}, the activation free energy (eq 3) becomes[13]

$$\Delta G^{\ddagger} = \frac{kT(\lambda + \Delta G^{\circ})^2}{2\sigma^2} \tag{5}$$

where $\sigma^2 = \langle (X - X_{min})^2 \rangle$, *i.e.*, the mean-square fluctuations of X, which may also easily be calculated from the simulation. Equation 5 will be referred to as the Gaussian fluctuation approximation.

B. Solvent Response Theory. In this section, the solvent free energy curves for reactions of infinitely separated solutes with a linear and a nonlinear response of a dielectric continuum solvent are described by two different simple models of ionic solvation, namely, the Born and HBI models, respectively. Details are given elsewhere,[13] so only the main points are summarized here.

In the limit where the donor and acceptor are at infinite distance apart, the electrostatic potentials at the donor and acceptor (eq 4) are independent so that the average polarization energies for the reactant and products are

$$\langle \Delta V \rangle_R = \langle \Phi_D(m) \rangle - \langle \Phi_A(n) \rangle$$
$$\langle \Delta V \rangle_P = \langle \Phi_D(m+1) \rangle - \langle \Phi_A(n-1) \rangle \quad (6)$$

the fluctuations of ΔV (assuming the tight binding approximation) are

$$\sigma^2 = \langle (\delta\Phi_D)^2 \rangle + \langle (\delta\Phi_A)^2 \rangle \quad (7)$$

where $\delta\Phi = \Phi - \langle\Phi\rangle$, and the solvent reorganization is

$$2\lambda = [\langle \Phi_D(m) \rangle - \langle \Phi_A(n) \rangle] - [\langle \Phi_D(m+1) \rangle - \langle \Phi_A(n-1) \rangle] \quad (8)$$

The solvent free energy can be cast in terms of the Born solvation energies of the donor and acceptor at infinite separation in a dielectric continuum solvent, which gives rise to Marcus theory. The Born approximation for electrostatic potential for an ion in solution is given by

$$\langle \Phi^{Born}(q) \rangle = \frac{-q}{R}\left(\frac{\epsilon - 1}{\epsilon}\right) \quad (9)$$

where q is the charge of the ion, R is the ion radius, and ϵ is the dielectric constant of the solvent, which shows the linear response. Moreover, the fluctuations in electrostatic potential can be shown to be[13]

$$\langle (\delta\Phi^{Born})^2 \rangle = \frac{k_B T}{R}\left(\frac{\epsilon - 1}{\epsilon}\right) \quad (10)$$

which is independent of q.

Thus, in the limit of infinite separation, the average polarization energies are[13]

$$\langle \Delta V \rangle_R = -\frac{m-n}{R}\left(\frac{\epsilon - 1}{\epsilon}\right), \quad \langle \Delta V \rangle_P = -\frac{m-n+2}{R}\left(\frac{\epsilon - 1}{\epsilon}\right) \quad (11)$$

The fluctuations in the polarization are

$$\sigma^2 = \frac{2k_B T}{R}\left(\frac{\epsilon - 1}{\epsilon}\right) \quad (12)$$

The latter shows that the fluctuations of the products and reactants are equal, as assumed by Marcus theory, and any differences between the force constants describing the reactants and products must be the result of nonlinear effects. Furthermore, one can then show[13]

$$\lambda = \sigma^2/2k_B T \quad (13)$$

Equations 5 and 13 give rise to the Marcus relation (eq 1). Finally, the free energy of solvation of the reactants versus the products is

$$\Delta G^\circ_{sol} = -\frac{m-n+1}{R}\left(\frac{\epsilon - 1}{\epsilon}\right) \quad (14)$$

The HBI model describes the interaction between an ion and a given molecule of the solvent as the interaction between a point charge and a dipole in a cavity, respectively, which are immersed in a dielectric continuum.[14] The solvation potential in this model is

$$\langle \Phi^{HBI}(q) \rangle = -4\pi\rho\boldsymbol{\mu} \int_R^\infty dr \langle \cos\gamma \rangle_r \quad (15)$$

where ρ is the number density of the solvent, R is the solute radius, and γ is the angle between the dipole vector and coordinate vector. For the HBI model,

$$\langle \cos\gamma \rangle_r = L[\beta\mu q/\epsilon' r^2] \quad (16)$$

where β is $1/k_B T$, μ is the dipole moment, ϵ' is the effective dielectric response,[14] and $L(x)$ is the Langevin function

$$L(x) = \coth(x) - 1/x \quad (17)$$

Thus, the HBI model is a quasi-continuum model and maintains the nonlinearity of the solvent response by retaining the full Langevin expression for the average orientation of polar molecules. The fluctuations in Φ are

$$\langle \delta\Phi^{HBI}(q) \rangle = \frac{1}{2q} k_B T[-\Phi^{HBI}(q) + 4\pi\rho\mu RL(\beta\mu q/\epsilon' R^2)] \quad (18)$$

The free energy curves from HBI theory are generated as described previously,[14] using the relation obtained by Zhou and Szabo[23]

$$\Delta G_R(X) = -\zeta X + \Delta G_{0\zeta}$$
$$\Delta G_P'(X) = (1-\zeta)X + \Delta G_{0\zeta} \quad (19)$$

where ζ is the charging parameter for a hypothetical state such that X corresponds to the minimum energy of that state. In this hypothetical state, ζ is a fraction of electronic charge transferred from the donor to the acceptor so that the charge is $m + \zeta$ and $n - \zeta$ for the donor and acceptor, respectively. Therefore, $\zeta = 0$ and $\zeta = 1$ correspond to the reactants and products, respectively. $\Delta G_{0\zeta}$ is the free energy change between the state 0 and the state ζ and is given by[13]

$$\Delta G_{0\zeta} = [S(n-\zeta) + S(m+\zeta) - S(n) - S(m)] + {}^2/_3[E(n-\zeta) + E(m+\zeta) - E(n) - E(m)] \quad (20)$$

where

$$S(q) = \frac{4\pi\rho\epsilon' R^3}{3\beta} \ln\left(\frac{\sinh(\beta\mu q/\epsilon' r^2)}{\beta\mu q/\epsilon' r^2}\right) \quad (21)$$

$$E(q) = q\langle \Phi^{HBI}(q) \rangle \quad (22)$$

C. Simulation. The molecular dynamics simulations were carried out using the molecular mechanics/dynamics package CHARMM 22g2 and CHARMM 24a3.[24] The energy parameters for the waters were from the TIP3P model.[25] Lennard-Jones parameters for iron ($\sigma_{FeO} = 2.53$ Å, $\epsilon_{FeO} = -1.2$ kcal/mol for the FeO interaction only)[7] were used to study the +2/+3 charge states and for sodium[26] ($\sigma_{NaO} = 2.72$ Å, $\epsilon_{NaO} = -0.13385$ kcal/mol; $\sigma_{NaH} = 1.31$ Å, $\epsilon_{NaH} = \epsilon_{NaO}$) were used to study the −1/0/+1 charge states. The simulations were for the systems in the microcanonical ensemble at a temperature of approximately 300 K. The Verlet algorithm was used to propagate the dynamics using a time step of 1 fs. All oxygen−hydrogen covalent bonds were held to their equilibrium bond lengths using the SHAKE algorithm. A constant dielectric of 1 was used throughout the simulation, and no electronic polarization was included.

For the isolated iron simulations and all solute paired simulations the atom based force shift[27] with a cutoff of 14 Å was used to approximate the electrostatic interactions. A cutoff distance of 15 Å was used for the nonbonded lists and image lists. The nonbonded lists were updated by the heuristic updating procedure, while the image lists were updated every 20 steps. The simulation of the solvated positively charged sodium ion was that of Hyun *et al.*[14] The simulations of the solvated uncharged and negatively charged sodium used the same conditions used by Hyun *et al.* For these simulations the group-based energy switch[24] was used in which the energy was switched smoothly to zero between 14 and 16 Å. A cutoff distance of 17.5 Å was used for the nonbonded lists and image lists. The nonbonded lists were updated by the heuristic updating procedure, while the image lists were updated every 50 steps.

All of the simulations used truncated octahedral periodic boundary conditions. Each system was prepared by placing the solute(s) in a preequilibrated truncated octahedral box of TIP3P waters. The dimensions of the box for the lone iron ions was 35 Å by 35 Å by 35 Å and contained 717 water molecules. The box dimensions for the lone sodium ions and all solute paired systems was 39.9 Å by 39.9 Å by 39.9 Å and containing 1062 or 1059 water molecules, respectively.

The initial equilibration of each simulation consisted of assigning velocities (according to a Gaussian distribution every 200 fs) to the solvent only for 3−5 ps while keeping the solute fixed. For the simulations of lone solute ions, velocities were assigned for another 3−5 ps to the whole system, but for the paired solute systems the ions were kept at a fixed distance from each other. Following assignment, the velocities were allowed to scale every 200 fs if the temperature was less than 295 K or greater than 305 K until there was no scaling for at least 5.0 ps. The amount of scaling ranged from 1.2 to 25 ps, depending on the system. Starting from at least 5.0 ps after the last velocity scale, the analysis portion consisted of dynamics in which the system was not perturbed saving the coordinates every 10 fs.

To construct free energy surfaces, the probability $P(X)$ in eq 2 is calculated by making a histogram of X obtained in a simulation. However, it is impractical to generate a full free energy curve from a molecular dynamics simulation because thermal fluctuations are generally not sufficient to allow sampling far away from $P(X_{\min})$. Non-Boltzmann or "umbrella" sampling[5,7,28] was used to obtain the free energy surface away from $X = X_{\min}$, in which the nuclear rearrangement due to intermediate values of charge on the two redox centers, meaning that the charge density of the transferring electron is $-(1 - z)e$ on one center and $-ze$ on the other. The probability in the system of interest (*i.e.*, for the reactants, $z = 0$) can be obtained from the probability in the intermediate system z via

$$P(\Delta V) = c^{(z)} e^{\beta z \Delta V} P^{(z)}(\Delta V) \tag{23}$$

where $X = \Delta V$, $c^{(z)}$ is a normalization constant, and $P^{(z)}$ indicates the probability when the system has the charge distribution characterized by z. A special case of umbrella sampling is when $z = 1$, so that $c^{(1)} = c^{(0)}$; thus, the left hand side of ΔG^{p} is given by $\Delta G^{\mathrm{R}} + \Delta V$, and the right hand side of ΔG^{R} is given by $\Delta G^{\mathrm{p}} + \Delta V$.[3,12] For both self-exchange reactions at close separations, simulations were carried out for $z = 0$, 0.25, and 0.50. Simulations for $z = 0.75$ and 1.00 were not needed due to the symmetry of the reactions. For the asymmetric charge recombination reaction at close separations, simulations were carried out for $z = 0$, 0.125, 0.25, 0.375, 0.5, 0.625, 0.75, 0.875, and 1.0. For symmetric reactions at infinite separations, the simulations were carried out only for $z = 0$ (and thus 1.0), and for asymmetric reactions at infinite separations, the simulations were carried out only for $z = 0$ and 1. The simulations of $z = 0$ and 1 consisted of 50 ps for the analysis portion, and the simulations of intermediate values of z consisted of 30 ps.

The polarization energy of X from the simulation requires the calculation of solvation energies (eq 4), which have large contributions from solvent far from the solute. The neglect of this contribution greatly affects the polarization energies for the simulations of the isolated ions. Therefore, the Born approximation for electrostatic potential (eq 7) was used to approximate the contribution of solvent beyond the cutoff distance (14 Å), using a dielectric constant of 68. The model of water used here (TIP3P) is very similar to SPC water,[29] which has been shown to have a dielectric constant of around 68, and is thus expected to be a reasonable dielectric constant. For solute−solute pairs separated by a finite distance, the contributions of solvent beyond the cutoff distance is small[7] because beyond the boundaries of simulation, the polarization energy due to the solute pair is essentially the same as that of a point charge.

Results

Three reactions are studied here: the $Fe^{2+} + Fe^{3+} \rightarrow Fe^{3+} + Fe^{2+}$ exchange reaction, the $Na^0 + Na^+ \rightarrow Na^+ + Na^0$ exchange reaction and the $Na^- + Na^+ \rightarrow Na^0 + Na^0$ charge recombination reaction. The ions were named on the basis of the Lennard-Jones parameters used to describe them in the simulation, so the reactions do not all reflect physically reasonable reactions. In particular, the "$Na^- + Na^+$" charge recombination is not a realistic system, but the results are present because they exemplify an asymmetric reaction and charge recombination reactions have been shown to have the largest saturation effects.[13] The choice of the same Lennard-Jones parameters for both ions simplifies the Born and HBI analysis. Moreover, the choice of sodium parameters was motivated by the observation that smaller radii enhance the saturation effects[13] and there is no singly charged negative ion of similar diameter. Thus, this system is meant to illustrate the types of changes in asymmetric reaction since they are magnified by the small radius and also to show that these changes are very large only when the radii of the ions are very small.

Results from MD simulations of the solutes at infinite and closely separated distances, referred to as MD(∞) and MD-(close), respectively, are shown, as are results from the HBI and Born model of solutes at infinite separation. The latter sets of results are shown not as a test of their predictive ability, but rather as an aid in explaining the physical origins of the solvation free energy curves. For both the Born and HBI results, the radius R was chosen to be the ionic radius (*i.e.*, $R = 0.64$ for Fe and $R = 0.97$ for Na), which will be discussed further in the Discussion.

A. Activation Energy. For free energy curves of the general shape shown in Figure 1, three features determine the activation energy $\Delta G^{\ddagger}$: the position of the minimum (*i.e.*, the average polarization energies, $\langle \Delta V \rangle$, of the reactants and products), the shape of the curve (*i.e.*, the width and the degree of nonparabolic behavior), and the overall free energy of the reaction, ΔG°. The latter is composed of both the intrinsic ionization potentials of the solutes and the free energies of solvation of the reactants versus the products, $\Delta G^{\circ}_{\mathrm{sol}}$, so all $\Delta G^{\ddagger}$ presented here assume that $\Delta G^{\circ} = \Delta G^{\circ}_{\mathrm{sol}}$ for simplicity. Of course, $\Delta G^{\circ}_{\mathrm{sol}} = 0$ for the self-exchange reactions. The solvation free energy curves for the three reactions were calculated from the HBI model for an infinitely separated pair (eqs 15, 16, and 19−22), the MD

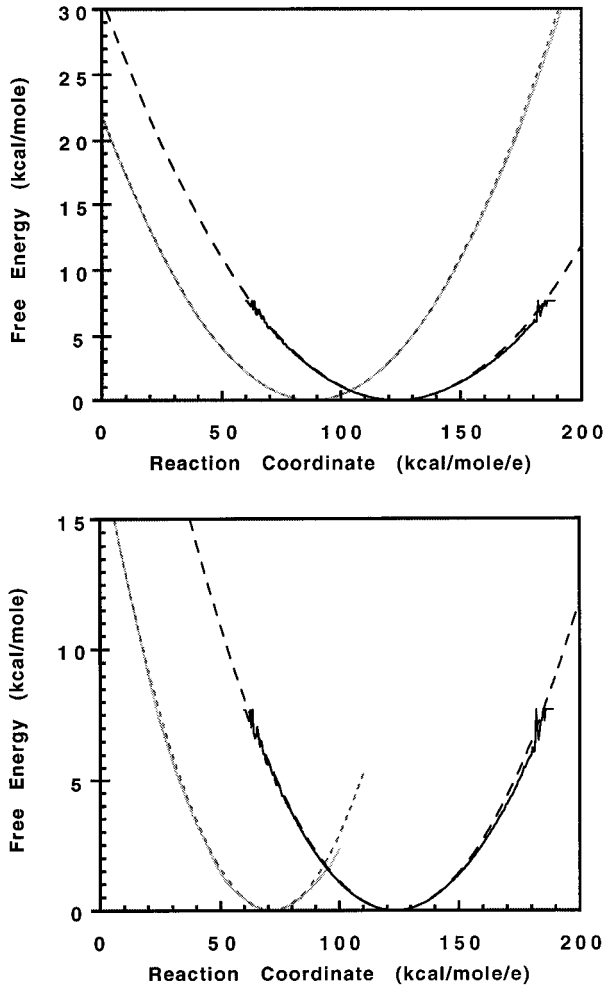

Figure 2. Free energy surfaces for the $Fe^{2+}-Fe^{3+}$ self-exchange reaction calculated from (a, top) HBI theory (solid gray line) and simulation of infinitely separated solutes (solid dark line) and (b, bottom) simulation of infinitely (solid dark line) and closely (solid gray line) separated solutes. The dashed lines represent the corresponding Marcus curves.

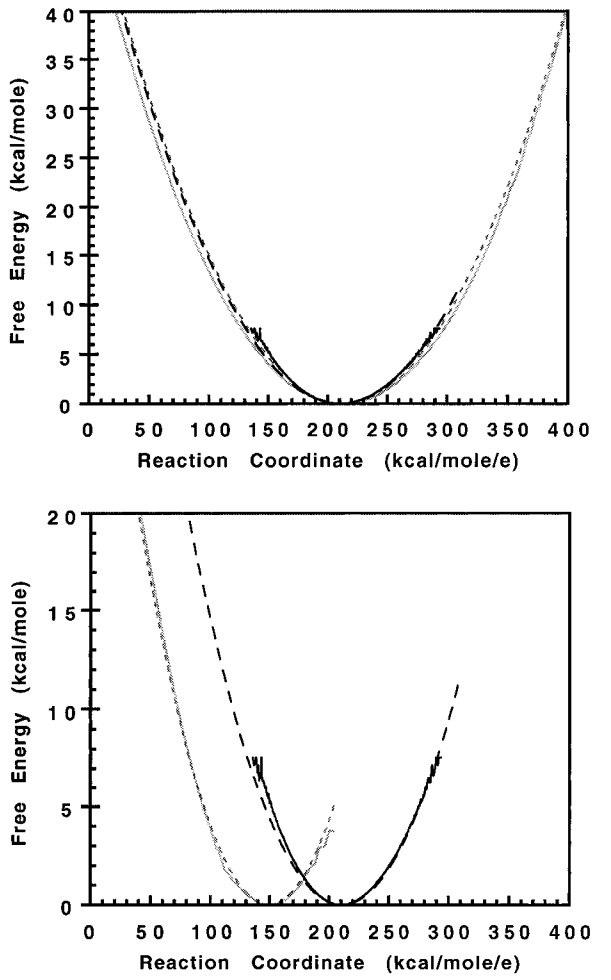

Figure 3. Free energy surfaces for the Na^0-Na^+ self-exchange reaction calculated from (a, top) HBI theory and simulation of infinitely separated solutes and (b, bottom) simulation of infinitely and closely separated solutes. Key as in Figure 2.

simulation of the infinitely separated pair, and the MD simulation of the closely separated pair (Figures 2−5). The latter two types of curves were calculated using histograms of the MD data and eq 2.

Activation energies were calculated using the Born (eqs 1, 13, and 14) and HBI (eqs 15, 16, and 19−22) models and from the crossing points of the calculated curves from the MD(∞) and MD(close) simulations (Table 1). For MD(∞), the $\Delta G^{\ddagger}$ are calculated by interpolating between the $z = 0$ and 1 surfaces. The results indicate considerable variation in the activation energy, which is from both the position of the minimum and the deviation from parabolic behavior. The Born model significantly overpredicts MD(∞), whereas the HBI model is relatively good. Furthermore, the MD(∞) activation energy is considerably higher than the MD (close) one.

B. Minima of the Solvent Free Energy Curves. The minima of the solvent free energy curves, or $\langle \Delta V \rangle$, for the reactants were calculated using the Born (eq 11) and HBI (eqs 6 and 15) models and the simulations at infinite and close separations (Table 1). In each case, the Born model overestimated and the HBI was close to or underestimated the MD(∞) results. MD(close) was always much smaller than the MD(∞) results. Since $\langle \Delta V \rangle = \langle \Phi_D \rangle - \langle \Phi_A \rangle$, the solvation energies of the donor and acceptor, $\langle \Phi_D \rangle$ and $\langle \Phi_A \rangle$, respectively, were also examined (Table 1). The Born values were consistently too high, whereas the HBI ones were somewhat comparable to MD(∞). Interestingly, the MD(∞) and MD(close) results differ more in the relative magnitudes of the donor and acceptor rather than the absolute magnitudes.

TABLE 1: Solvation Electrostatic Potentials (kcal/mol/*e*), Polarization Energies (kcal/mol), and Activation Free Energies (kcal/mol), Calculated from the Born Approximation, HBI Theory, Simulations of the Single Ions, MD(∞), and Simulations of the Paired Ions, MD(close)

solute pair	$\langle \Phi_D \rangle$	$\langle \Phi_A \rangle$	$\langle \Delta V \rangle$	$\Delta G^{\ddagger}$
$Fe^{2+}-Fe^{3+}$				
Born	−1086	−1628	543	136
HBI	−349	−437	88	22
MD(∞)	−383	−506	123	∼30
MD(close)	−426	−497	71	18
Na^0-Na^+				
Born	0	−358	358	90
HBI	0	−213	213	50
MD(∞)	1	−210	211	∼55
MD(close)	−32	−181	149	39
Na^--Na^+				
Born	358	−358	716	358
HBI	213	−213	426	249
MD(∞)	334	−210	544	∼316
MD(close)	269	−152	421	208

To investigate the structural basis for the nonlinear effects, the contribution to the total solvation potential Φ of a given solute was calculated for shells of solvent around the solute in the different oxidation states (Table 2). In all cases, it is apparent that the deviation of the Born and HBI results from the MD(∞) results are due to the solvation within the first 6 Å,

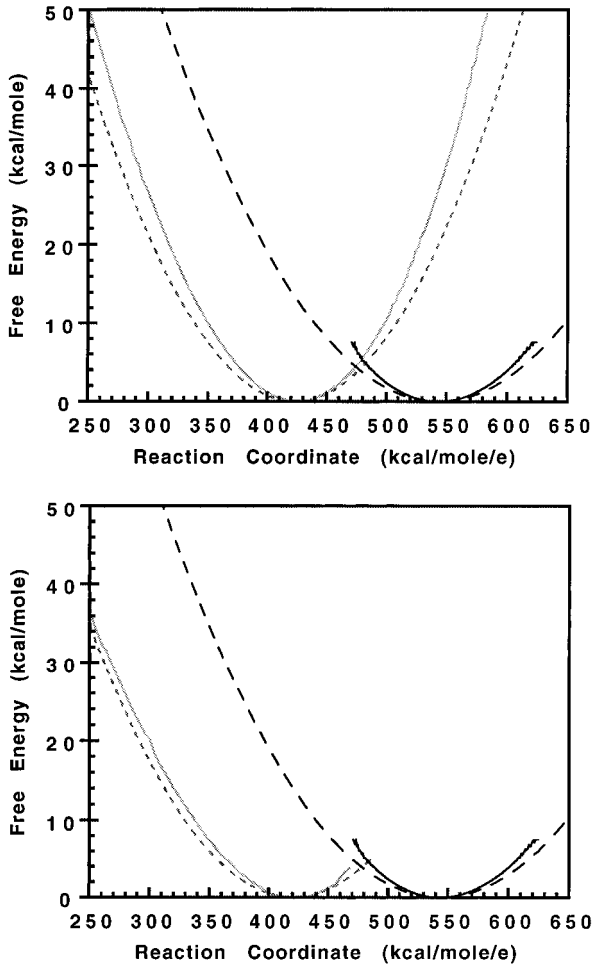

Figure 4. Free energy surfaces for the $Na^{-}-Na^{+}$ reactants in the charge recombination reaction calculated from (a, top) HBI theory and simulation of infinitely separated solutes and (b, bottom) simulation of infinitely and closely separated solutes. Key as in Figure 2.

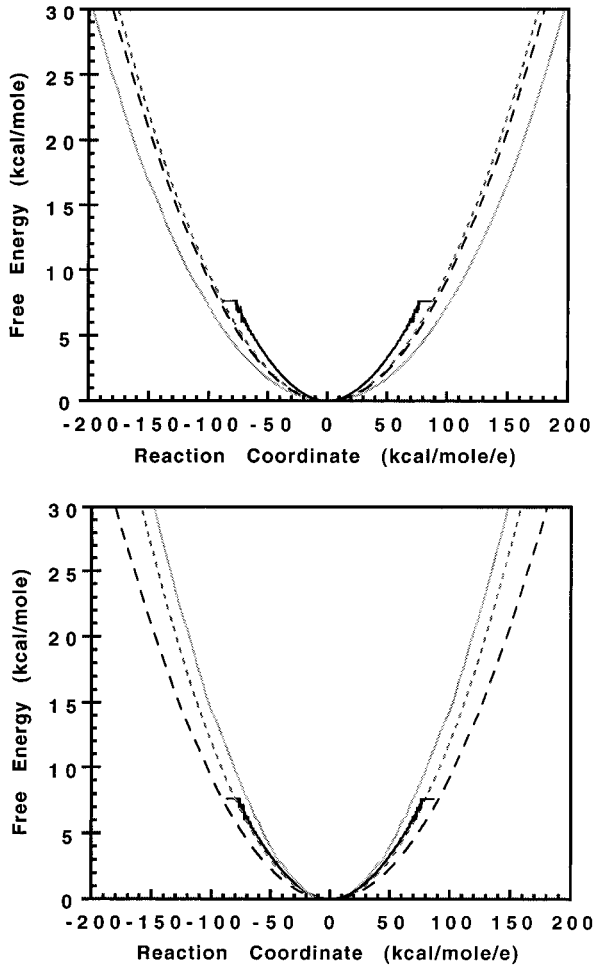

Figure 5. Free energy surfaces for the $Na^{0}-Na^{0}$ products in the charge recombination reaction calculated from (a, top) HBI theory and simulation of infinitely separated solutes and (b, bottom) simulation of infinitely and closely separated solutes. Key as in Figure 2.

which corresponds to the first two solvation shells. However, between the MD(∞) and MD(close) results, the first 6 Å is very similar but the difference appears in the 6−12 Å range. In addition, the ratios of the potentials of one oxidation state *m* to another state *n* indicate the degree of nonlinearity due to each shell, with ideal linear behavior indicated by a ratio of *m*/*n* as shown by the Born results (Table 2). For the $Fe^{2+}-Fe^{3+}$ system, HBI and MD(∞) showed considerable deviation from 1.5 in the first 6 Å, but the response became more linear after the first shell, while for the $Na^{-}-Na^{+}$ system, only MD(∞) showed a large deviation from −1 for the first 6 Å and did not approach linear behavior until after 10 Å. On the other hand, for both $Fe^{2+}-Fe^{3+}$ and $Na^{-}-Na^{+}$, MD(close) had approximately the same ratio as MD(∞) for the first 6 Å, but the ratio beyond 6 Å approached 1.

TABLE 2: Comparison of Contributions of Shells to Average Solvation Potentials (kcal/mol/*e*) and Ratios of Contributions to Solvation Potentials, Calculated from the Born Approximation, HBI Theory, Simulations of the Single Ions, MD(∞), and Simulations of the Paired Ions, MD(close)

shell (Å)	Born	HBI	MD(∞)	MD(close)
$\Phi_{Fe^{2+}}$				
0.0−6.0	−970	−235	−283	−297
6.0−12.0	−58	−57	−50	−116
$\Phi_{Fe^{3+}}$				
0.0−6.0	−1454	−268	−354	−359
6.0−12.0	−87	−83	−77	−125
$\Phi_{Fe^{3+}}/\Phi_{Fe^{2+}}$				
0.0−6.0	1.5	1.14	1.25	1.21
6.0−12.0	1.5	1.47	1.55	1.07
$\Phi_{Na^{-}}$				
0.0−6.0	300	156	274	267.4
6.0−12.0	29	29	32	1.2
$\Phi_{Na^{+}}$				
0.0−6.0	−300	−156	−154	−153
6.0−12.0	−29	−29	−28	−1.0
$\Phi_{Na^{+}}/\Phi_{Na^{-}}$				
0.0−6.0	−1.0	−1.0	−0.56	−0.57
6.0−12.0	−1.0	−1.0	−0.88	→1[a]

[a] The potential at each becomes vanishingly small so the ratio approaches 1.

C. Shape of the Solvation Free Energy Curves. The nonlinearity of each of the curves in Figures 2−5 is illustrated by a Marcus-type parabola centered at the same minimum as the respective curve and with a width determined by eq 12. In other words, different effective radii for each of the curves from HBI, MD(∞), and MD(close) were obtained via eq 11, and then those radii were used in eq 12 to obtain σ^2 for the parabola. Thus, these "Marcus" curves differ from the Born curves in that no physical information (*i.e.*, the radii of the ions) is included in the Marcus curves, whereas the Born curves use the ionic radii, but otherwise the equations are the same.

Another indicator of nonparabolic behavior is seen in the calculation of the activation energies using the Marcus relation (eq 1) and the Gaussian fluctuation approximation (eq 5), referred to as $\Delta G^{\ddagger}_{M}$ and $\Delta G^{\ddagger}_{G}$, respectively (Table 3), rather than the crossing point of the curves in Figure 2. The deviations from parabolic (linear) behavior can be measured by the ratio

TABLE 3: Activation Free Energies (kcal/mol) Defined as in Table 1[a]

reaction	$\Delta G^{\ddagger}_{M}$	$\Delta G^{\ddagger}_{G}$	$\Delta G^{\ddagger}_{M}/\Delta G^{\ddagger}_{G}$
$Fe^{2+}-Fe^{3+}$			
HBI	22	22	1.01
MD(∞)	31	30	1.05
MD(close)	18	15	1.20
$Na^{0}-Na^{+}$			
HBI	53	46	1.16
MD(∞)	53	58	0.91
MD(close)	37	52	0.72
$Na^{-}-Na^{+} \rightarrow 2Na^{0}$			
HBI	213	330	0.65
MD(∞)	136	362	0.38
MD(close)	105	244	0.43

[a] $\Delta G^{\ddagger}_{M}$ was calculated using the Marcus relation; $\Delta G^{\ddagger}_{G}$ was calculated using the Gaussian fluctuation approximation.

TABLE 4: Fluctuations in Φ ($\langle \delta\Phi_X^2\rangle^{1/2}$ (kcal/mol/*e*), X = D,A) for the Donor and Acceptor, Fluctuations in Δ*V* (*σ* (kcal/mol)), and the Solvent Reorganization Energies (*λ* (kcal/mol)) Calculated from HBI Theory, the Simulations for the Ions at Infinite Separation, MD(∞), and for the Simulations of the Closely Paired MD(close) Ions

solute pair	$\langle \delta\Phi_D^2\rangle^{1/2}$	$\langle \delta\Phi_A^2\rangle^{1/2}$	σ	λ
$Fe^{2+}-Fe^{3+}$				
HBI	7.6	6.9	10.3	88
MD(∞)	9.0	8.5	12.4	123
MD(close)	9.2	8.7	10.1	71
$Na^{0}-Na^{+}$				
HBI	14.6	9.0	17.1	213
MD(∞)	10.5	10.8	15.1	211
MD(close)	11.0	11.3	14.4	149
$Na^{-}-Na^{+}$				
HBI	9.0	9.0	12.8	249
MD(∞)	11.1	10.8	15.6	∼316
MD(close)	11.7	11.6	14.7	208
$Na^{0}-Na^{0}$				
HBI	14.6	14.6	20.6	177
MD(∞)	10.5	10.5	15.2	∼325
MD(close)	11.1	11.5	14.0	216

$\Delta G^{\ddagger}_{M}/\Delta G^{\ddagger}_{G}$, which should be 1 if the solvent response is truly linear (eqs 1, 5, and 13). For the infinite separation case, for both HBI and MD(∞), $Fe^{2+}-Fe^{3+}$ is the most linear and the charge recombination is the least linear. Also, $\Delta G^{\ddagger}_{M}/\Delta G^{\ddagger}_{G}$ was further from 1 for MD(close) than for MD(∞), in all but the $Na^{-}-Na^{+}$ reaction.

The contributing factors to $\Delta G^{\ddagger}_{M}$ and $\Delta G^{\ddagger}_{G}$ are functions of the average properties of the polarization energies ΔV and thus Φ (Table 4). For the Fe simulations, the fluctuations $\langle \delta\Phi^2\rangle$, decrease with increasing charge. However, $\langle \delta\Phi^2\rangle$ around the uncharged sodium atom was smaller than for either of the charged sodium ions in MD(∞) and were comparable in MD-(close), in contrast with the HBI results. The reasons for this discrepancy are discussed later. Another source of nonlinearity in the MD(close) results is that σ^2 is less than $\langle \delta\Phi_D^2\rangle + \langle \delta\Phi_A^2\rangle$, indicating that the fluctuations in the solvent potentials of the donor and acceptor are correlated.

Discussion

Here, the infinite separation MD simulations are discussed in terms of the Born and HBI models to understand how the solvation free energy differs from the simple Born model. Next, the closely paired MD simulations are compared with the infinite separation simulation to understand the influence of one solute on the polarization of the other. Deviations from Marcus curves are discussed in terms of the physical origins of the deviation and how they affect the curves. Nonlinearity of the solvent response, whatever the physical origin, can be manifested by nonlinear changes of $\langle \Phi\rangle$ with charge and thus shifts in $\langle \Delta V\rangle$, nonconstant $\langle \delta\Phi^2\rangle$ with charge and thus unequal σ for the curves, and nonparabolic curves.

A. Infinite Separation. The simplest models of solvation studied here are the Born and HBI models, both of which are used to describe the solvation of two infinitely separated solutes in a dielectric continuum. We have previously discussed the comparison of the solvation free energy curves for these two models thoroughly,[13] so the purpose of including them both here is that the deviation of the HBI from the Born model for a solute of radius *R* demonstrates the contribution of dielectric saturation to changing the Born curves. This is because, in the HBI model, the solvent energy is described in terms of the average orientation of the solvent molecules ($\cos\gamma$), which is a Langevin function of the electric field $E = q/\epsilon' r^2$ (eq 16). As the field increases, $|\langle\cos\gamma\rangle_r|$ "saturates" at a maximum possible value of 1 so that the solvent molecules cannot orient any more and the solvation energy can no longer increase; thus, the response is nonlinear with respect to *E*. However, the Born model can be obtained by a Taylor expansion of the Langevin function,[14] implying that $|\langle\cos\gamma\rangle_r|$ is directly proportional to *E* and thus can increase without bound, which is of course not possible for the cosine function. Moreover, this implies that the solvation energy is directly proportional to *E* and so the response is linear.

The simulations of the ions at infinite separation include various molecular effects not included in the HBI model. For instance, electrostriction due to the interaction between the charge and the water dipoles leads to compression of the solute cavity and/or greater density of solvent around the ion with increasing charge of the ion. In addition, for the negative ions, there are other components besides electrostriction. For instance, there is a breakdown of the dipole approximation for the solvent in the first shell[13] because the preferred orientation of the water around a negative ion is with one hydrogen forming a linear hydrogen bond to the ion. Also, the effective radius of a negative ion is smaller than that of a positive ion because the center of the water dipole moment is able to come closer to the negative ion since, although the oxygens are approximately equidistant from the positive and negative ions, the hydrogens are closer to the negative ion than to the positive ion.

For the purpose of comparison to the MD results, the ionic radii of Fe^{2+} and Na^{+} are chosen for *R* in both the HBI and the Born calculations. Since the variation from Born (or HBI) occurs only close to the ion (Table 2), it is possible to choose an effective radius (*i.e.*, the "Born radius") to account for any possible effects such as dielectric saturation, electrostriction, and the molecular nature of the solvent. However, since the point here is to identify such effects, the same ionic radius is used for both the Born and HBI models. In other words, the Born results are for an ion of radius *R* (with no electrostriction) in a linear response, constant density solvent, and the HBI results are for an ion of the same radius *R* (with no electrostriction) in a nonlinear response, constant density solvent, with the nonlinear response due to dielectric saturation. Because of this, differences between the two are only due to dielectric saturation so that the contributions of dielectric saturation independent of other effects can be estimated.

For the infinite separation case, the $\Delta G^{\ddagger}$ from Born, HBI, and MD(∞) vary mainly due to differences in the average polarization energy $\langle \Delta V\rangle$ (Table 1). There is a large decrease in $\Delta G^{\ddagger}$ (and $\langle \Delta V\rangle$) in all of these reactions between the Born and HBI results, reflecting the effects of dielectric saturation. Since $\langle \Phi_D\rangle$, $\langle \Phi_A\rangle$, and $\langle \Delta V\rangle$ of MD(∞) are more similar in magnitude to those of HBI rather than those of Born, this implies the MD(∞) results also show effects of dielectric saturation;

thus, dielectric saturation appears to reduce $\Delta G^{\ddagger}$ by between 40 to 110 kcal/mol. There are, however, variations between HBI and MD(∞), reflecting deviations due to the molecular nature of the solvent in the MD results, which lead to an increase in $\Delta G^{\ddagger}$.

The influence of the various effects on the solvation can be understood further by examining the contributions to Φ per shell for the different solutes (Table 2). For $Fe^{2+}-Fe^{3+}$, the ratio of Φ_A/Φ_D deviates from the linear values of 1.5 in the first 6 Å but not in the next 6 Å for MD(∞) and HBI, implying similar (but not identical) effects of dielectric saturation. In other words, the MD(∞) and the HBI results show evidence of saturation near the ion where the field is strongest. The magnitude of the contribution of the first shell for Fe^{3+} and Fe^{2+} in MD(∞) is considerably smaller than that from Born, also reflecting dielectric saturation. However, it is larger than that from HBI, which can be attributed mainly to the local density around a charged species being both larger and closer, reflecting electrostriction. For Fe^{2+} and Fe^{3+}, the density variation is especially important since it is not possible to obtain good values for $\langle\Phi\rangle$ using HBI even by reducing R nor for $\langle\Delta V\rangle$ by adjusting the relative sizes of Fe^{2+} and Fe^{3+} by a physically reasonable amount (results not shown). On the other hand, for $Na^{-}-Na^{+}$, the ratio of Φ_A/Φ_D for MD(∞) not only deviates from the linear values of 1.0 in the first 6 Å (but not in the next 6 Å), but also from the HBI model, which also gives a value of 1.0 for all shells since HBI does not differentiate between negative and positive ions. In fact, the magnitude of Φ for Na^{+} in MD(∞) is predicted better by HBI than by Born, reflecting dielectric saturation. However, for Na^{-} in MD(∞), the additional factors for negative ions (breakdown of dipole approximation and closer dipole center) also come into play.

The nonlinearity of the solvent response is also manifested in the fluctuations (Table 4). The HBI results for all of the reactions show the expected nonlinear response, that the more highly charged solutes have smaller $\langle\delta\Phi^2\rangle$ since the higher the charge, the more restricted the solvent should be around the solute.[9−11,13] Since the HBI model differs from the Born model only by including dielectric saturation, the changes in $\langle\delta\Phi^2\rangle$ in HBI must be due to dielectric saturation. The MD(∞) results also show that $\langle\delta\Phi^2\rangle$ decreases with increasing charge for $Fe^{2+}-Fe^{3+}$, indicating dielectric saturation here as well; in contrast, the $\langle\delta\Phi^2\rangle$ for the Na^0 are smaller than those of either Na^{-} or Na^{+}. This discrepancy can be attributed to a decrease in the effective solute radius when the charge of the Na is increased, an electrostriction effect, leading to larger fluctuations, since the Born approximation for solvation potential predicts that the fluctuations are inversely proportional to the radius (eq 8). Since the fluctuations are larger for the singly charged Na than for the neutral, the effect of electrostriction is apparently larger than the dielectric saturation effect for the uncharged and singly charged ions.

The results for the solvation free energy curves of the HBI model and the MD(∞) model for the solutes at infinite separation show that, for $Fe^{2+}-Fe^{3+}$ (Figure 2) and $Na^{-}-Na^{+}$ (Figure 4), the MD(∞) results deviate from their respective Marcus curve in the same fashion as the HBI results deviate from their respective Marcus curve. This is also illustrated by the similar ratios of $\Delta G^{\ddagger}_M/\Delta G^{\ddagger}_G$ for the HBI and MD(∞) results (Table 3). The deviations from the Marcus curves are very small for $Fe^{2+}-Fe^{3+}$ and are much more striking for the various Na reactions, as we previously predicted from the HBI model.[13]

On the other hand, the HBI and MD(∞) results differ for the Na^0-Na^{+} (Figure 3) and Na^0-Na^0 (Figure 5) curves, as seen in both the deviation from the respective Marcus curves and the $\Delta G^{\ddagger}_M/\Delta G^{\ddagger}_G$ values (for Na^0-Na^{+} only in Table 3). This is because σ is smaller with respect to its Marcus value for MD(∞) than for HBI; *i.e.* $\Delta G^{\ddagger}_M/\Delta G^{\ddagger}_G = \sigma^2/2k_BT\lambda$ is smaller for MD(∞) than for HBI. The reason σ for MD(∞) is small is in part due to the small $\langle\delta\Phi^2\rangle$ predicted for Na^0, since the effective radius for a neutral ion in the MD is larger than for a charged ion and thus the fluctuations are small compared to HBI, where the radii are constant and are based on the ionic radius of Na^{+}. This also affects the $Na^{-}-Na^{+}$ reaction, but here by reducing the $\Delta G^{\ddagger}_M/\Delta G^{\ddagger}_G$ ratio, the net change is to make the deviation from Marcus even more pronounced than HBI, since HBI already predicts $\Delta G^{\ddagger}_M/\Delta G^{\ddagger}_G < 1$ for this reaction.

The net effects are that dielectric saturation leads to smaller increases in $\langle\Phi\rangle$ and decreases in $\langle\delta\Phi^2\rangle$ with increasing charge and that electrostriction leads to larger increases in $\langle\Phi\rangle$ and increases in $\langle\delta\Phi^2\rangle$ with increasing charge, which are competing effects. The presence of a negative rather than a positive ion further reduces the effective ionic radius so that there are also larger increases in $\langle\Phi\rangle$ and larger $\langle\delta\Phi^2\rangle$. The variation in $\langle\delta\Phi^2\rangle$ reflects the nonparabolicity of the curve and the unequal curvatures for the reactants and products.[13] In the $Fe^{2+}-Fe^{3+}$ reaction, the major effects of dielectric saturation and electrostriction are on $\langle\Delta V\rangle$, with very little effect on the shape of the curve. For the Na^0-Na^{+} reaction, the dielectric saturation affects $\langle\Delta V\rangle$ and it is not possible to see how electrostriction affects $\langle\Delta V\rangle$ since the polarization of Na^0 is zero. However, both dielectric saturation and electrostriction affect the shape of the curve in opposing directions, with the electrostriction dominating. For the $Na^{-}-Na^{+}$ reaction, dielectric saturation, electrostriction, and the negative/positive ion effective radius difference affect $\langle\Delta V\rangle$ and the curvature. For the reactants, the decrease in fluctuations due to dielectric saturation are only slightly cancelled by the increase in fluctuations due to electrostriction, so the MD(∞) and HBI curves relative to the respective Marcus curves look similar. However, for the products, the increase in fluctuations due to the dielectric saturation are dominated by the decrease in the fluctuations due to the lack of electrostriction around the Na^0, so the net fluctuations are smaller.

B. Infinite Separation versus Finite Separation. The major effect on $\Delta G^{\ddagger}$ of the second solute on the first when the solutes are at close separations is due to smaller average polarization energies when the reactants are close to one another (Table 1). This is because if they are infinitely separated, all of the solvent responds to a net change in charge, whereas if the reactants are close together, only the solvent near the solutes reorganized appreciably whereas the bulk solvent essentially sees the net charge of the two solutes, which does not change during the reaction. Therefore, the closer together the solutes are to one another, the less reorganization there will be by the bulk solvent so that in the limit when they occupy the same place, there will be no reorganization. This can be seen in that the shell contributions Φ_D and Φ_A become essentially identical for large r (*i.e.*, $\Phi_A/\Phi_D \rightarrow 1$) for both the $Fe^{2+}-Fe^{3+}$ and the $Na^{-}-Na^{+}$ pairs and correspond to the solvation energy of a charge of +5 and 0, respectively (Table 2): *i.e.*, $\langle\Delta V\rangle$ is smaller for MD(close) than for MD(∞) due to solvent beyond 6 Å. Hence, the closer the solutes come to one another, the lower the activation barrier (Table 1), as was observed in simulations of the $Fe^{2+}-Fe^{3+}$ self-exchange reaction by Kuharski *et al.*[7] and as was also discussed previously by Yelle and Ichiye.[30] An interesting observation is that the contribution within 6 Å to Φ for a given solute is very similar between MD(∞) and MD(close), indicating that changes in the inner shell solvent has a relatively small effect on the differences in $\langle\Delta V\rangle$ between MD-

(close) and MD(∞). In other words, although most of $\langle \Delta V \rangle$ in MD(close) is due to inner solvent since the bulk solvent does not change during the reaction, the inner shell solvation of closely paired solutes is fairly well represented by the inner shell solvation of infinitely separated solutes.

The solvation curves of MD(close) are also generally more nonlinear than those of MD(∞) as measured by $\Delta G^{\ddagger}_{M}/\Delta G^{\ddagger}_{G}$ (Table 3), which can be attributed to both the changes in $\langle \Phi \rangle$ noted above and to nonlinear effects on the solvent fluctuation. The fluctuations in the solvation potential Φ are generally larger for the closely paired systems than those of the isolated systems. However, in all cases the fluctuations in the polarization energies, σ^2, are smaller for the MD(close) than for the MD(∞) systems, because since the polarization energies are correlated for the closely paired systems, the fluctuations are also correlated.

Conclusions

The effects of dielectric saturation, electrostriction, and molecular structure play different roles on the activation energies of different reactions. On the whole, for ions at infinite separation, it appears that $\Delta G^{\ddagger}$, is affected mainly by shifting the minimum (and reducing the width of the curve) as reflected by the change in $\langle \Delta V \rangle$ between Born and HBI (Table 1). The effect on $\Delta G^{\ddagger}$ of the nonparabolic nature of curve as demonstrated by $\Delta G^{\ddagger}_{M}/\Delta G^{\ddagger}_{G}$ and by the shifts relative to the "Marcus" curves is much smaller, except for the extreme case of $Na^{-}-Na^{+}$ charge recombination. Including electronic polarization will affect $\langle \Delta V \rangle$ both by the electronic shielding and by the enhanced polarization of the solvent molecules near the ion, so care must be taken in including its effects.

For the $Fe^{2+}-Fe^{3+}$ exchange reaction, the net effect of dielectric saturation is small on the shape of the MD(∞) solvation free energy curves, as has been noted in the HBI model.[13] Molecular effects also do not cause a significant deviation from parabolic behavior. The major differences between MD(∞) and the Born model are a very large reduction in $\Delta G^{\ddagger}$ due to a large increase in $\langle \Delta V \rangle$ from dielectric saturation and a small increase in $\Delta G^{\ddagger}$ due to a small decrease in $\langle \Delta V \rangle$ from the increased density of solvent near the highly charged solutes, a molecular effect.

The reactions involving the Na-like ions are less physically realistic systems but demonstrate the small diameters necessary to have large effects. For these systems, the effects of dielectric saturation are much more apparent in the shape of the MD(∞) curves as predicted earlier for the HBI model[13] of this system. In addition, two molecular factors influence the MD(∞) curves: the effective radius of Na^0 is larger than Na^+ or Na^- due to the lack of the charge−dipole attraction, and the effective radius of Na^- is smaller than Na^+ because the center of the water dipole moment can approach closer to Na^-. In the Na^0-Na^+ reaction, the major difference between MD(∞) and the Born model appears to be due to dielectric saturation, which causes a large decrease in $\langle \Delta V \rangle$ and also should increase the fluctuations for Na^0-Na^+ relative to the $Na^{1/2}-Na^{1/2}$ state (making the curve nonparabolic), thus reducing $\Delta G^{\ddagger}$. However, the increase in fluctuations for Na^0-Na^+ relative to $Na^{1/2}-Na^{1/2}$ due to dielectric saturation is apparently more than cancelled by the decrease in fluctuations due to a change in the effective radius, thus slightly increasing $\Delta G^{\ddagger}$. For the $Na^{-}-Na^{+}$ reaction, the differences between MD(∞) and the Born model are a large reduction in $\Delta G^{\ddagger}$ due to a decrease in $\langle \Delta V \rangle$ from dielectric saturation counterbalanced by an increase in $\Delta G^{\ddagger}$ due to an increase in $\langle \Delta V \rangle$ from the effective radius of the negative and positive ions. The deviations from Marcus parabolas are influenced by two competing factors: the decrease in fluctuations around charged ions due to dielectric saturation and the decrease in fluctuations around the neutral ion due to its increased effective radius, resulting in $Na^{-}-Na^{+}$ MD(∞) curves dominated by dielectric saturation and thus resembling HBI and Na^0-Na^0 MD(∞) curves dominated by the size differences.

Finally, the large drop between the infinitely separated and the closely separated $\Delta G^{\ddagger}$ is due to less reorganization of the bulk solvent, which greatly reduces λ. The direct influence of one solute on the polarization of the other is to increase the nonlinearity of the curve, but the effect on $\Delta G^{\ddagger}$ is rather small.

Acknowledgment. We would like to thank Attila Szabo and Jin-Kee Hyun for helpful discussions. This work was supported by grants from the National Institutes of Health (1R29 GM45303) and the National Science Foundation (MCB-9118085 and MCB-9506796). We would also like to thank the Maui High Performance Supercomputing Center and the VADMS Center at Washington State University for computational resources.

References and Notes

(1) Marcus, R. A.; Sutin, N. *Biochim. Biophys. Acta* **1985**, *811*, 265−322.
(2) Levich, V. G. *Adv. Electrochem. Electrochem. Eng.* **1966**, *4*, 349−371.
(3) Warshel, A. *J. Phys. Chem.* **1982**, *86*, 2218−2224.
(4) Churg, A. K.; Weiss, R. M.; Warshel, A.; Takano, T. *J. Phys. Chem.* **1983**, *87*, 1683−1694.
(5) Hwang, J.-K.; Warshel, A. *J. Am. Chem. Soc.* **1987**, *109*, 715−720.
(6) King, G.; Warshel, A. *J. Chem. Phys.* **1990**, *93*, 8682−8692.
(7) Kuharski, R. A.; Bader, J. S.; Chandler, D.; Sprik, M.; Klein, M. L.; Impey, R. W. *J. Chem. Phys.* **1988**, *89*, 3248−3257.
(8) Chandler, D.; Kuharski, R. A. *Faraday Discuss. Chem. Soc.* **1988**, *85*, 329−340.
(9) Kakitani, T.; Mataga, N. *Chem. Phys.* **1985**, *93*, 381−397.
(10) Kakitani, T.; Mataga, N. *Chem. Phys. Lett.* **1986**, *124*, 437−441.
(11) Carter, E. A.; Hynes, J. T. *J. Phys. Chem.* **1989**, *93*, 2184−2187.
(12) Tachiya, M. *J. Phys. Chem.* **1989**, *93*, 7050−7052.
(13) Ichiye, T. *J. Chem. Phys.* **1996**, *104*, 7561−7571.
(14) Hyun, J.-K.; Babu, C. S.; Ichiye, T. *J. Phys. Chem.* **1995**, *99*, 5187−5195.
(15) Kim, H. J.; Hynes, J. T. *J. Chem. Phys.* **1991**, *96*, 5088−5110.
(16) Kim, H. J. *J. Chem. Phys.* **1996**, *105*, 6818−6832.
(17) Gehlen, J. N.; Chandler, D.; Kim, H. J.; Hynes, J. T. *J. Phys. Chem.* **1992**, *96*, 1748−1753.
(18) Dang, L. X.; Rice, J. E.; Caldwell, J.; Kollman, P. A. *J. Am. Chem. Soc.* **1991**, *113*.
(19) Rick, S.; Stuart, S. J.; Berne, B. J. *J. Chem. Phys.* **1994**, *101*, 6141.
(20) Dang, L. X. *J. Chem. Phys.* **1992**, *97*, 2659.
(21) Warshel, A.; Russel, S. T. *Q. Rev. Biophys.* **1994**, *17*, 283−422.
(22) Zhu, S. B.; Singh, S.; Robinson, G. W. *Adv. Chem. Phys.* **1994**, *90*.
(23) Zhou, H.-X.; Szabo, A. *J. Chem. Phys.* **1995**, *103*, 3481−3494.
(24) Brooks, B. R.; Bruccoleri, R. E.; Olafson, B. D.; States, D. J.; Swaminathan, S.; Karplus, M. *J. Comput. Chem.* **1983**, *23*, 327−341.
(25) Jorgensen, W. L. *J. Am. Chem. Soc.* **1981**, *103*, 335−340.
(26) Dang, L. X.; Pettit, B. M. *J. Phys. Chem.* **1990**, *94*, 4303−4308.
(27) Steinbach, P. J.; Brooks, B. R. *J. Comput. Chem.* **1994**, *15*, 667−683.
(28) Valleau, J. P.; Torrie, G. M. A Guide to Monte Carlo for Statistical Mechanics: 2. Byways. In *Modern Theoretical Chemistry*; Berne, B. J., Ed.; Plenum: New York:, 1977; Vol. 5, p 137.
(29) Belhadj, M.; Alper, H. E.; Levy, R. M. *Chem. Phys. Lett.* **1991**, *179*, 13−30.
(30) Yelle, R. B.; Ichiye, T. *J. Phys. Chem.*, submitted for publication.